CFD Simulation of Air-water Film Flow for Reactor Vessel Upper Downcomer Using VOF-slip Model

Chi-Jin Choi and Hyoung Kyu Cho *
Nuclear Thermal-Hydraulic Engineering Laboratory, Seoul National University
1 Gwanak-ro, Gwanak-gu, Seoul 08826
**Corresponding author:chohk@snu.ac.kr*

1. Introduction

The computational fluid dynamics (CFD) has come to occupy an important position in nuclear reactor safety analyses that require accurate prediction of 3D geometrical effects for two-phase flow. A small-scale flow processes that are not seen by system codes can be accessed with CFD, which would result a better estimation of safety margins [1]. In this sense, the liquid film behavior at reactor vessel (RV) upper downcomer is worthwhile subject to investigate with CFD. During the reflood phase of a loss of coolant accident (LOCA) in APR1400, subcooled emergency core cooling (ECC) water is injected into the downcomer through the direct vessel injection (DVI) nozzle. Then, the ECC water impinges on the core barrel wall and flows downward in the form of liquid film. In the meantime, circumferential steam flow from the intact cold legs to the broken cold leg is formed and interacts with liquid film. The interfacial friction between phases generates wisps and droplets from the liquid film and they lead to ECC water bypass to the broken cold leg.

Several two-phase CFD models such as Volume of Fluid (VOF), two-fluid approach, and mixture approach have been developed to predict multiphase flow behavior. However, each of the traditional models is known for providing relatively reliable outcomes only for one of the dispersed or segregated flows [2], which is not appropriate to model the ECC bypass phenomenon. Another challenge in CFD simulation is concerned with modeling turbulence in large-scale interface. It is known that high velocity gradients near the interface generates unphysical turbulence, especially in eddy-viscosity models of Reynolds-averaged Navier-Stokes (RANS) approach [3]. Because this causes large discrepancies in terms of velocity and pressure drop near the free surface, additional damping of turbulence is required [4].

This paper aims at validating CFD simulation of air-water film flow in the 1/10 reduced-scale RV downcomer. In order to address above issues, the present study utilized VOF-slip model, one of hybrid models combining VOF and mixture approaches implemented in STAR-CCM+ v13.02 [5]. This approach enables the large-scale interface to be treated with VOF and the subgrid-scale interface to be treated with mixture model. In addition, Egorov model [4] was introduced with SST $k-w$ turbulence model to damp the turbulence at the interface. The simulation results were validated with experiment data including local liquid film thickness and ECC bypass fraction [6].

2. Air-water Film Flow Simulation

2.1. VOF-slip model

The VOF model as an interface capturing method is suitable for describing free surface flow, where the interface length is larger than the mesh size. However, the model is not capable of describing dispersed phase flow, where the interface length is smaller than the mesh size because one velocity field is shared between the phases in VOF method. On the other hand, the mixture model does not capture the interface but it accounts for phase slip velocity via drag law so that the model is capable of describing dispersed phase flow.

The VOF-slip is a hybrid model combining the VOF and the mixture models, which can treat the large-scale interface and small-scale interface simultaneously. In VOF-slip model, diffusion velocity terms are added in the volume fraction transport equation and momentum equation of VOF model. The diffusion velocity, $\mathbf{v}_{d,i}$ means the difference between phase velocity and mass-averaged velocity, and it can be expressed with phase slip velocity v_{ps} as follows:

$$\frac{\partial \alpha_i}{\partial t} + \nabla \cdot (\alpha_i \mathbf{v}) = -\frac{1}{\rho_i} \nabla \cdot \left(\alpha_i \rho_i \mathbf{v}_{d,i}\right) \quad (1)$$

$$\frac{\partial (\rho \mathbf{v})}{\partial t} + \nabla \cdot (\rho \mathbf{v}\mathbf{v}) = -\nabla \mathbf{p} + \rho \mathbf{g} + \nabla \cdot \boldsymbol{T} + \mathbf{f_s} + \nabla \cdot \sum \alpha_i \rho_i \mathbf{v}_{d,i} \mathbf{v}_{d,i} \quad (2)$$

$$\mathbf{v}_{d,p} = \left(\frac{\alpha_p \rho_p}{\rho} - 1\right) \mathbf{v}_{ps} \quad (3)$$

$$\mathbf{v}_{ps} = C_D \mathbf{b} \quad (4)$$

where C_D is the drag coefficient provided by the Schiller-Naumann model, and $\mathbf{b}$ is specific body forces. The Schiller-Naumann drag coefficient assumes that the primary phase is continuous and the secondary phase is dispersed, which are defined as:

$$C_D = C_D^{ps} = \frac{\tau_s}{f_{drag}^{ps}} \frac{(\rho_s - \rho)}{\rho_s} \quad (5)$$

$$\tau_s = \frac{\rho_s d_s^2}{18 \mu_p} \quad (6)$$

$$f_{drag}^{ps} = \begin{cases} 1 + 0.15 Re_{ps}^{0.687} & \text{if } Re_{ps} \le 1000 \\ 0.0183 Re_{ps} & \text{if } Re_{ps} > 1000 \end{cases}, \; Re_{ps} = \frac{\rho_p |\mathbf{v}_{ps}| d_s}{\mu_p} \quad (7)$$

Although C_D is determined with droplet diameter d_s, there is no available reference diameter obtained from the experiment. Therefore, sensitivity analysis of droplet diameter was conducted to confirm the proper diameter that can predict reasonable bypass fraction with experiment result.

2.2. Interface turbulence damping

One of the most widely used way of damping the interface turbulence is to apply Egorov [4] model. In this model, a source term is added in the w equation of the $k-w$ model, which enhances the specific turbulence dissipation rate as follows:

$$S_i = A_i \cdot \Delta n \beta \rho_i \left(\boldsymbol{B} \frac{6\mu_i}{\beta \rho_i \Delta n^2} \right)^2 \quad (8)$$

This source term is only activated in the interfacial region by introducing an indicator A_i. As a damping coefficient **B** increases, the specific dissipation rate increases, which makes eddy viscosity decreases. Thus, to determine **B** is crucial for predicting the free surface behavior that is affected by the interfacial friction. However, there has been no general guideline for the selection of **B** in the previous studies [7]. In most cases, **B** used to be tuned to predict the experiment results well. In the present study, the effect of **B** on the simulation results were investigated and the trend of **B** that gives reasonable results at each case was confirmed.

2.3. Computational domain and simulation cases

The test section in air-water film flow experiment [6] was modeled as shown in Fig. 1. There are two intact cold legs for air inlet and a broken cold leg for air-water outlet. DVI nozzle is placed above the broken cold leg and the water is injected through this nozzle. The bottom of the domain is set as a water outlet, which controls the water out flow rate to keep the water level constant. The trimmed meshes were used and total number of the elements is approximately 6,200,000. The simulation conditions are presented in Table 1.

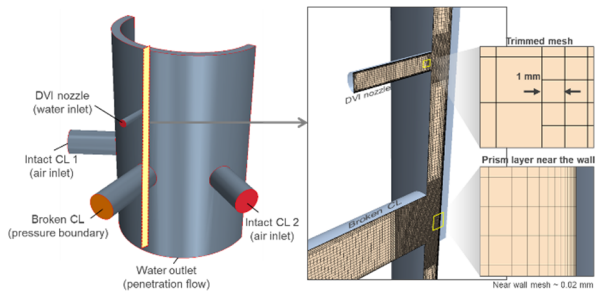

Fig. 1. Computational domain and mesh configuration

Table 1: Simulation conditions

Water inlet velocity	Re_f		v_f [m/s]
	2.32×10^4		0.63
	3.28×10^4		0.89
Air outlet velocity	$Re_{g,o}$		$v_{g,o}$ [m/s]
	Low	1.00×10^5	20
		1.10×10^5	22
	High	1.20×10^5	24
		1.30×10^5	26
		1.40×10^5	28

3. Results and Discussion

3.1. No air flow conditions

In the case of no air flow, transient simulation with time step of 0.2 ms was conducted as shown in Fig. 2. The film interface was expressed by iso-surface of void fraction at 0.5. In the simulation, the injected water from DVI nozzle impinges on the wall and spreads in the form of the liquid film.

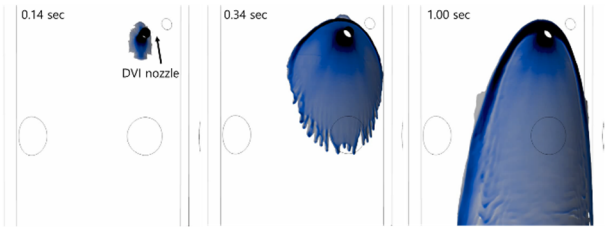

Fig. 2. Transient simulation results (W089A00)

The spatio-temporal averaged film thickness was compared with experiment results in Fig. 3. The CFD could predict the thick film boundary and the spreading width of liquid film reasonably. Figure 4 shows the comparison result of liquid film thickness. Although film thickness at film boundary region was underestimated, overall film thickness was comparable; VOF method could properly capture the film interface behavior under no air flow conditions.

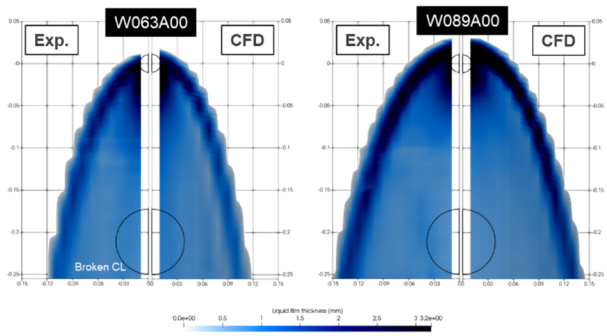

Fig. 3. Comparison of liquid film distribution (W063A00, W089A00)

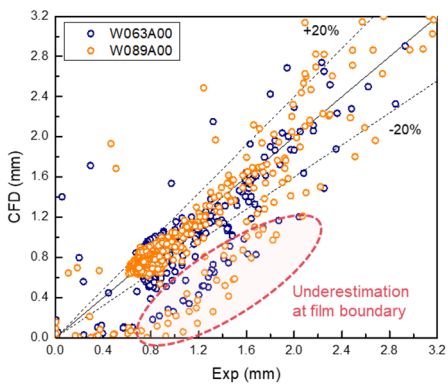

Fig. 4. Comparison of liquid film thickness (W063A00, W089A00)

3.2. Air flow conditions

In the case of air injection from the two intact cold legs, spreading width of liquid film becomes narrower toward the broken cold leg and the entrainment occurs from the liquid film. Then, the unresolved droplet flow starts to contribute to ECC bypass toward the broken cold leg, which is affected by the slip velocity estimation. To assess the effect of droplet diameter on the phase slip velocity, sensitivity analysis of droplet diameter was conducted under low air flow condition (W063A20). The reason for performing the analysis under low air flow condition is to minimize the effect of film boundary position on the bypass fraction. Figure 5 shows phase slip velocity at the broken cold leg with different droplet diameter. As the droplet diameter increases, magnitude of phase slip velocity increases according to the eqns. (4)-(7). This indicates that velocity of unresolved droplet becomes slower as increasing droplet diameter. Accordingly, the ECC bypass fraction decreases with using large droplet diameter as shown in Fig. 6. When the VOF model is applied, the bypass fraction was overestimated about three times because the phase slip was not considered. Based on the fact that the droplet diameter of 20 μm in VOF-slip model could predict the most accurate bypass fraction result in this condition, droplet diameter of 20 μm was used for all simulation cases.

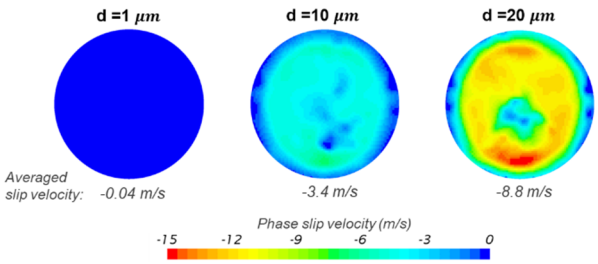

Fig. 5. Phase slip velocity with different droplet diameter (W063A20)

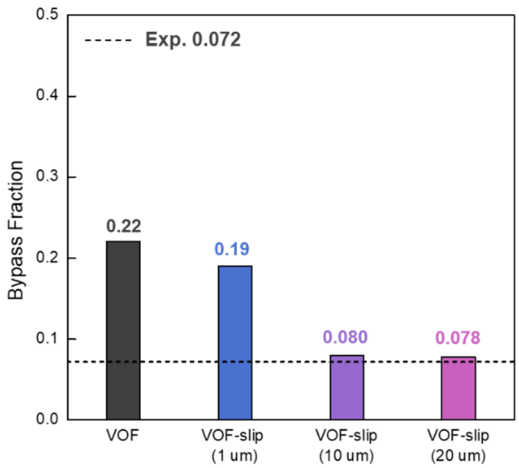

Fig. 6. Bypass fraction with different droplet diameter (W063A20)

Under the high air flow conditions, the spreading width of liquid film became much narrower and the thick liquid film was formed near the cold leg. Strong air flow toward the broken cold leg made thickened film stretched and generates wisps (see Fig. 7.). This implies that not only the unresolved droplet behavior but also the liquid film and wisps behaviors are major factors affecting ECC bypass under high air flow conditions. Those free surface behaviors are closely related to the interfacial friction, which might have to be reduced with Egorov damping model. Thus, the effect of the damping coefficient **B** on the simulation results was investigated.

Figure 8 shows the changes of film spreading width with different **B**. As **B** increases, spreading width of the liquid film near the broken cold leg becomes wider due to the reduced interfacial friction. By the use of **B**=20, CFD could predict the most comparable film boundary to the experiment result in W063A26 case (see Fig. 9).

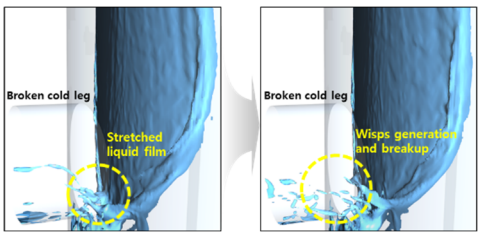

Fig. 7. Thickened liquid film and wisps generation near the broken cold leg under high air flow condition (W063A26).

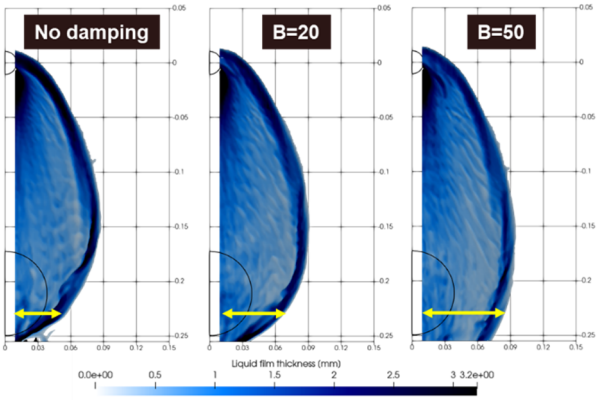

Fig. 8. Changes of film spreading width with different **B** (snapshot in W063A24)

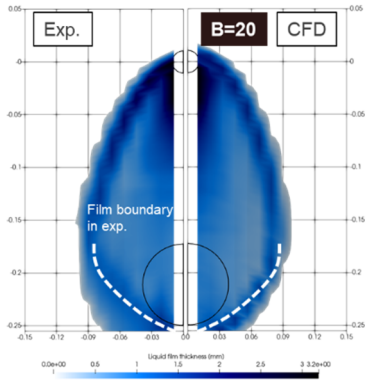

Fig. 9. Comparison of film spreading width with **B=20** (W063A24)

The effect of **B** on the bypass fraction is shown in Fig. 10. When the turbulence is not damped at the film interface, the overestimated interfacial friction makes spreading width of liquid film excessively narrow, which causes large error in predicting bypass fraction. It is worth noting that calculated bypass fraction with **B**=20 is the most comparable to the experiment result. This means that accurate simulation of free surface behavior by adopting proper **B** lead to reliable prediction of bypass fraction as well. Table 2 shows the selection of **B** for each simulation case, which can predict the bypass fraction and spreading width of liquid film well at the same time. The bypass fraction in all simulation cases was compared in Fig. 11. In most cases, CFD could predict comparable bypass fraction except for W089A20 and W089A22. The large discrepancy in both cases might be caused by the use of constant droplet diameter (20 **μm**). Therefore, further investigations are required about the way of introducing the reasonable droplet diameter value in the simulation.

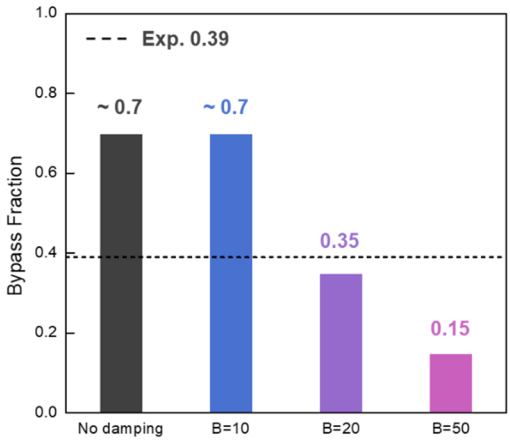

Fig. 10. Bypass fraction with different B (W063A24)

Table 2: Selection of B for each simulation case

	No damp	B=20	B=40
W063A20	○		
W063A22	○		
W063A24		○	
W063A26			○
W063A28			○
W089A20	○		
W089A22	○		
W089A24		○	
W089A26		○	
W089A28		○	

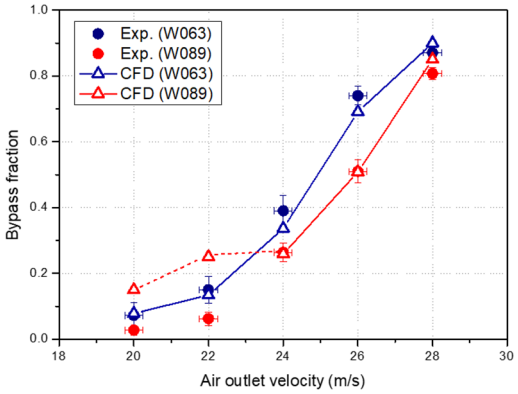

Fig. 11. Comparison of bypass fraction in all simulation cases

4. Conclusion

The air-water film flow at RV upper downcomer was simulated using the STAR-CCM+ code. For proper modeling of free surface (liquid film and wisp) flow and dispersed (droplet) flow, the VOF-slip model was introduced. The effect of droplet diameter on the slip velocity was confirmed and the dimeter was decided based on the bypass fraction result. Under high air flow conditions, the effect of interface turbulence damping on the simulation results was investigated as well. By the use of proper damping coefficient, spreading width of liquid film and water bypass fraction could be well matched with experiment results. The reason for large discrepancy in bypass fraction under low air flow conditions should be further investigated.

ACKNOWLEDGMENT

This work was supported by the National Research Foundation (NRF) of Korea funded by the MSIP (No. NRF-2018M2B2A906574423/0666-20210004).

REFERENCES

[1] D. Bestion, Extension of CFD codes application to two-phase flow safety problems, Nuclear Engineering and Technology, Vol. 42, No. 4, pp. 365-376, 2010.
[2] M. Akhlaghi, V. Mohammadi, N. M. Nouri, M. Taherkhani, and M. Karimi, Multi-Fluid VOF model assessment to simulate the horizontal air-water intermittent flow, Chemical Engineering Research and Design, Vol. 152, pp. 48-59, 2019.
[3] T. Hohne and C. Vallee, Modelling of stratified two phase flows using an interfacial area density model, WIT Trans. Engineering Science, Vol. 63, pp. 123-133, 2009.
[4] Y. Egorov, M. Boucker, A. Martin, S. Pigny, M. Scheuerer, and S. Willemsen, Validation of CFD codes with PTS-relevant test cases, 5th Euratom Framework Programme ECORA project, pp. 91-116, 2004.
[5] STAR-CCM+ user guide, version 13.02, Siemens, 2018.
[6] C. J. Choi and H. K. Cho, Investigation on emergency core coolant bypass with local measurement of liquid film thickness using electrical conductance sensor fabricated on flexible printed circuit board, International Journal of Heat and Mass Transfer, Vol. 139, pp. 130-143, 2019.
[7] W. Fan, H. Anglart, Progress in Phenomenological Modeling of Turbulence Damping around a Two-Phase Interface, FLUIDS, Vol. 4, No. 3, pp. 136, 2019.